Effect of Vertical-Ejector Jet on the Aerodynamics of Delta Wings

Joseph Katz* and Dieter Kern†
San Diego State University, San Diego, California

The effect of adding a vertical jet to a 76-deg delta wing was investigated experimentally and theoretically in terms of the resulting longitudinal aerodynamic characteristics. A small-scale wind-tunnel experiment served for the investigation, and a simplified vortex lattice model was constructed to simulate the first-order effects of this complex flowfield. The major benefits of this combined approach over the use of more developed computer schemes lies in the relative ease in tailoring the mathematical model to a new problem. Results of both the wind-tunnel experiment and the theoretical model showed measurable lift loss due to the ejector jet throughout the whole angle-of-attack range, which will intensify at lower flight speeds.

Nomenclature

$\mathcal{R}$ = aspect ratio, wing area/b^2 = 1
b = wing span, 0.28 m
C_L = lift coefficient, lift/$0.5\rho V_\infty^2 S$
C_D = drag coefficient, drag/$0.5\rho V_\infty^2 S$
C_T = thrust coefficient, jet thrust/$0.5\rho V_\infty^2 S$
c = wing reference chord, 0.56 m
d = wing thickness, 0.02 m
dl = line element along a vortex line
F = aerodynamic force
H = vertical distance
Re_c = Reynolds number, based on wing's root chord
r = vector (x,y,z)
S = reference area, 0.0784 m^2
u,v,w = velocity components
V_{jet} = average velocity across ejector, 15 m/s
V_∞ = freestream velocity
x,y,z = coordinates
α = angle of attack
α_i = induced downwash angle at the center of the ith vortex element
Γ = circulation
Δt = time step used for wake rollup calculations
ρ = air density

Introduction

THE benefits of V/STOL (vertical and short takeoff and landing) capability for a variety of aircraft applications have been recognized for some time. Among the many V/STOL concepts[1,2] examined, one of the more competitive in achieving a multijet lifting system is the ejector-assisted lift augmentation. According to this concept, a primary jet nested in the wing planform propels additional air flow across and normal to the wing. If the aircraft must perform supersonic cruise and high-speed maneuvers, in addition to V/STOL, then the wing geometry will reflect this by having a considerable leading edge aft-sweep. Wings of this type develop a substantial portion of their total lift from vortex flow, which is generated by the separated vortices originating along the strakes and the wing leading edge. This additional vortex lift can be used during transition from vertical takeoff to forward flight, where large values of lift coefficient at low speed are required.

Many aspects of the interaction between lifting jets and lifting surfaces have been studied and examples are provided in Refs.1–7. The loss of lift due to these lifting jets, especially near the ground, was realized during early concept studies[1,3] that focused on level-flight and ground effect. High angle-of-attack, low-speed, jet-assisted, and out-of-ground effect flight conditions were not thoroughly studied in these references. However, during the transition of a V/STOL aircraft with highly swept wings, from forward flight to hover, such conditions will frequently be encountered. Therefore, for this study, a highly swept and sharp leading edge delta wing was selected

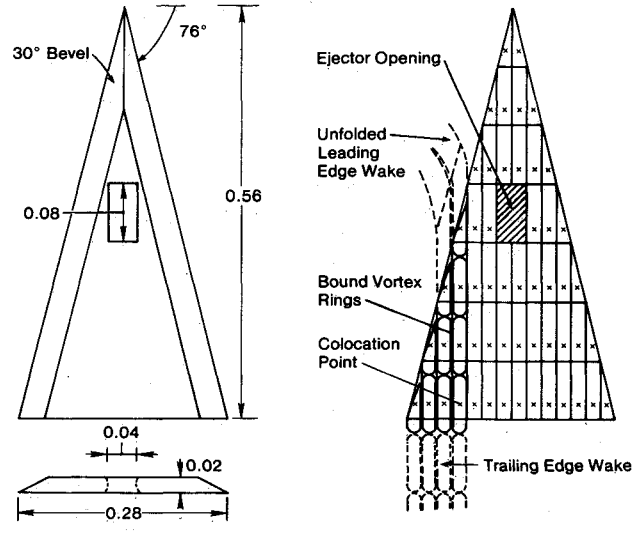

Fig. 1 Geometry of the delta wing (dimensions in meters) and its vortex-ring representation.

Presented as Paper 88-3842 at the 1st National Fluid Dynamics Congress, Cincinnati, OH, July 25–28, 1988; received Oct. 29, 1988; revision received Oct. 26, 1989.

*Professor, Department of Aerospace Engineering.
†Graduate Student, Department of Aerospace Engineering.

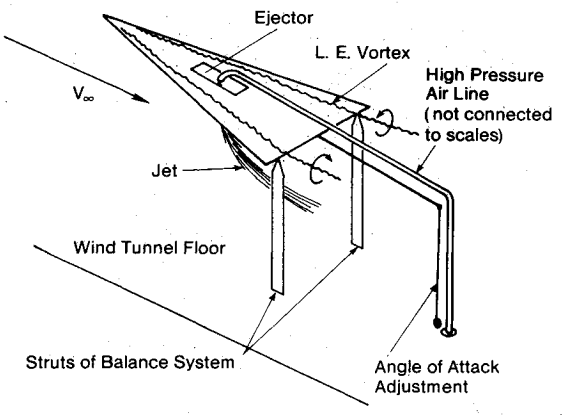

Fig. 2 Schematic description of wing and jet as mounted in the wind-tunnel test section.

so that the effect of the normal-jet induced flowfield on the high angle-of-attack and out-of-ground-effect aerodynamics could be isolated and investigated.

Experimental Apparatus

The geometry of the 76-deg delta wing ($\mathcal{R} = 1$) and the equivalent vortex-lattice model are presented in Fig. 1. The location and shape of the rectangular ejector opening was dictated by the simplified numerical model of the delta wing, which had a tip-to-tip grid of 14 × 7 panels. This ejector geometry is not representative of efficient ejector design and future studies should use better detailed and more efficient configurations. The low-speed, closed-return-type wind tunnel, which was used for the tests, had a cross section of 1.14 m × 0.81 m (45 × 32 in.) and was capable of speeds of up to 80 m/s. The wing was mounted on two struts at its trailing edge (see Fig. 2) that were attached to a scale beneath the wind tunnel. The scale is capable of measuring the lift and drag coefficient with a resolution that is better than 0.01. The wing's attitude was varied by a thin, long, central rod positioned behind the wing. The jet-induced flowfield was experimentally simulated by a single, elliptic, cross-section jet, in the middle of the rectangular opening in the wing. The high-pressure air supply was suspended in the tunnel and was not connected to the scales in order to isolate the vortex-induced effect from the thrust of the jet. The stagnation pressure of the air supply for the jet was about 5.5 atm (80 psi) and was held constant throughout the test. The compressed air was ejected through a converging elliptic nozzle (0.005 m × 0.015 m) and the axial velocity field due to the jet, in an undisturbed environment, and outside of the wind tunnel, is summarized in Fig. 3. The three curves represent the velocity profiles in meter/second, along straight survey lines at distances of 0.125, 0.250, and 0.500 m below the jet, as described in the inset in Fig. 3.

First-order corrections due to model support interference were made based on measuring the aerodynamic loads without the delta wing in the test section. Maximum wind-tunnel blockage, at the higher angles of attack, was on the order of 4.5%, and when the jet was "on," it was rapidly turned into the freestream, thus staying far from the wind-tunnel walls. Because of this small area ratio and because of the wing's small aspect ratio, wind-tunnel wall interference was not investigated and no lift or blockage corrections were applied to this experimental data.

Vortex Lattice Model

The combined fluid dynamic problem of lifting jets, leading-edge separation, and three-dimensional wing planform is highly complex and nonlinear. It is assumed here that the first-order effect of vortex lift and wake rollup can be estimated by incompressible fluid dynamic equations with full three-dimensional capability. This capability was demonstrated for simple delta-wing planforms when the nonlinear portion of the vortex lift was estimated and explained via simple vortex models.[8,9] In the current work, a computational method, based on a vortex-ring element,[8] was used to solve the three-dimensional flowfield. The first step in applying this method to a given wing geometry is establishing the computational grid, as shown in Fig. 1. Once the grid geometry is established, bound vortex rings are assigned to each panel, as shown in the figure. The leeward portion of the vortex is placed at the quarter chord of the panel element and its trailing segment is located in the quarter chord of the following panel. Therefore, the net circulation of each panel is the difference between the circulation of its bound vortex and of the trailing vortex of the adjacent forward panel. The triangular panel elements at the wing leading edge are treated as rectangular panels with coinciding side edges. The advantage of placing leeward segment of the vortex ring at the quarter chord of the panel (see Fig. 1) is that the lifting properties of the wing can be obtained by using a small number of such vortex rings. This was investigated in Ref. 8, where a grid of 5 chordwise × 10 spanwise vortex rings was found to be adequate. In the present case, a grid of 7 chordwise × 14 spanwise elements was used, which is sufficient for lift calculations and still economical on a VAX 780 computer (less than 1 min CPU/run).

In order to find the influence of a vortex ring element, the velocity ΔV induced by a dl-long vortex line segment is calculated by Eq. (1), along each of the four segments of each vortex ring.

$$\Delta V = \frac{-\Gamma}{4\pi} \int_{\text{vortex-line}} \frac{r \times dl}{r^3} \tag{1}$$

Since the vortex line is an elementary solution of the potential flowfield, the only boundary condition left is the one requiring that there be no flow through the solid-wing surface. This condition is satisfied at the center of the vortex rings (at the collocation points), as shown in Fig. 1. Adding the induced velocities of all the vortex elements in the field and enforcing the preceding boundary condition on the wing's surface results in the following integral equation.

$$V_\infty \alpha - V_{\text{jet}} - \frac{1}{4\pi} \int_{\text{wing + wake}} \Gamma_l \frac{r \times dl}{r^3} = 0 \tag{2}$$

Here the term V_{jet} was added to simulate the effect of a prescribed normal velocity across the wing solid boundaries, and n is a vector normal to the wing's surface. For the wing

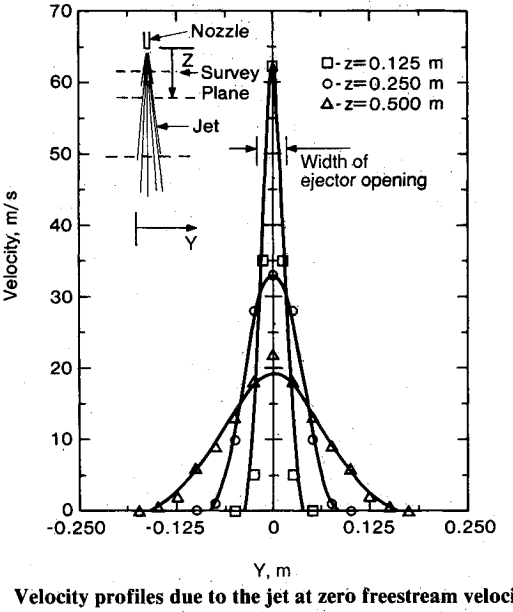

Fig. 3 Velocity profiles due to the jet at zero freestream velocity; z is the distance of the survey plane from the nozzle exit measured in meters.

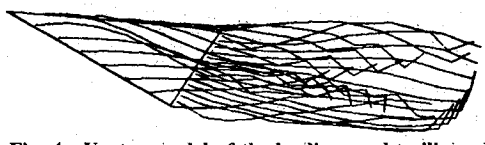

Fig. 4 Vortex model of the leading- and trailing-edge wakes after 15 steps (only longitudinal segments are shown since in this case of steady-state flow, the strength of the spanwise elements is zero).

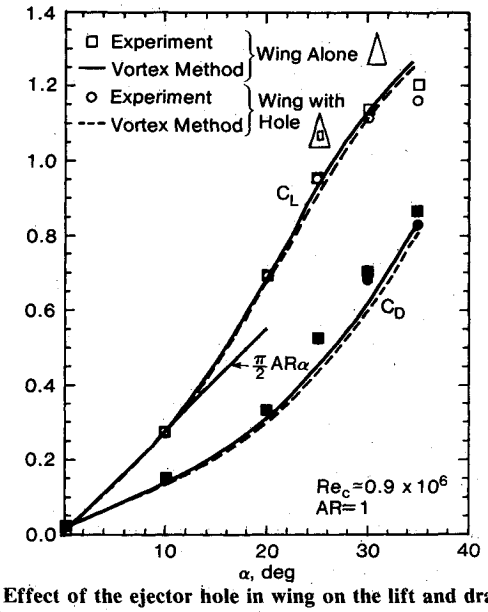

Fig. 5 Effect of the ejector hole in wing on the lift and drag of the delta wing; jet hardware is removed.

geometry described in Fig. 1, $V_{jet} = 0$ is used for all panels, except for those two representing the ejector. The experimental velocity distribution inside the ejector consisted of a small cross section but high speed jet at the middle of the rectangular opening (see Fig. 3), surrounded by a much slower outer flow. On the other hand, the vortex model of the ejector (vortex ring) results in higher velocities near the boundary and lower normal velocities at the ejector center. To compensate for this difference, the total mass flow rate across the ejector surface was assumed to be the same for both the experimental and the analytical calculations. Consequently, for the calculations, a representative $V_{jet} = 15$ m/s was specified at the center of the ejector panels (see Fig. 1), and the thrust coefficient was varied by varying the freestream velocity.

Equation (2), when specified for each of the k vortex-ring elements, results in a set of k linear, algebraic equations with $\Gamma_i (i = 1 \rightarrow k)$ as the unknown, which can be solved by standard matrix techniques.

The wake, shed at the wing trailing and leading edges, is represented by similar vortex-rings, and their strength is set equal to the strength of the corresponding wake shedding panel on the wing (Kutta condition). This principle of modeling wakes and leading edge vortices shed from highly swept wings is presented in detail in Ref. 8 (for thin) and in Ref. 9 (for thick delta wings). In the case of thin and sharp leading edges, as it is assumed here, the separation line is located along the leading edge (and almost insensitive to Reynolds number effects), and the computed aerodynamic coefficients are close to measured data (see Ref. 9).

In practice, the solution of Eq. (2) is obtained by a time-stepping method that starts with a wakeless solution. The time-marching technique, combined with Eq. (3) allows the wake elements to follow the local streamline direction[10] $(u,v,w)_i$, which actually means that there is no force on the wake element

$$\begin{pmatrix} \Delta x \\ \Delta y \\ \Delta z \end{pmatrix} = \begin{pmatrix} w \\ v \\ w \end{pmatrix}_i \cdot \Delta t \tag{3}$$

Here Δt is the iteration time step, Δt = panel chord/V_∞, and there is no distinction between leading edge, trailing edge, and jet wakes (which were simulated by convecting the jet enclosing vortex rings downstream[11]). The time-stepping procedure is continued until convergence is obtained (about 15 steps), and the results of such a wake rollup calculation are presented in Fig. 4.

Once the bound-vortex element strength Γ_i is computed, the aerodynamic force contribution ΔF_i of each panel is calculated by

$$\Delta F_i = \rho(V_{\infty i} + u) \times \Gamma_i \cdot \Delta y \tag{4}$$

where u_i is the x component of the local disturbance velocity. The aerodynamic coefficients are then obtained by integrating ΔF_i over the wing surface:

$$C_L = \frac{\sum_{i=1}^{k} \Delta F_i \cos\alpha_i^*}{0.5\rho V_\infty^2 S} \tag{5}$$

$$C_D = \frac{\sum_{i=1}^{k} \Delta F_i \sin\alpha_i^*}{0.5\rho V_\infty^2 S} \tag{6}$$

Here α_i^* represents an induced angle caused by the wing's spanwise vortex elements only, which locally distorts the direction of the freestream flow. Therefore, in order to have the lift perpendicular and the drag parallel to the freestream, the force ΔF_i of Eq. (4) is rotated by α_i^* relative to the direction, normal to V_∞ (this rotation affects mainly the induced drag calculations).

Results

Prior to the investigation of the jet-induced flow, the effect of the rectangular hole on the wing's longitudinal aerodynamics was investigated (see Fig. 5). Both calculated and measured data indicate that the effect is small, and the difference is noticeable only at the larger angles of attack ($\alpha > 25$ deg). This is probably a result of the flow across the hole, which may affect leading edge vortex burst; a phenomenon that cannot be estimated by the present vortex model. At the lower angle-of-attack range ($\alpha < 10$ deg), the effect of the leading edge vortex wake is small and was not included in the calculations (but at $\alpha = 10$ deg, it was included). Both the computed and the measured data in Fig. 5 lie close to the linear lift slope of $C_{L_\alpha} = (\pi/2)\mathcal{R}$, and thereby support this assumption. The beveled leading edge of the wind-tunnel model had a small effect (resulting

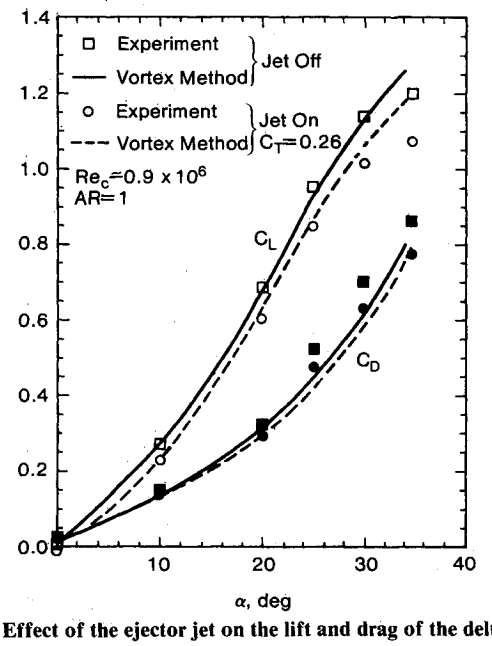

Fig. 6 Effect of the ejector jet on the lift and drag of the delta wing.

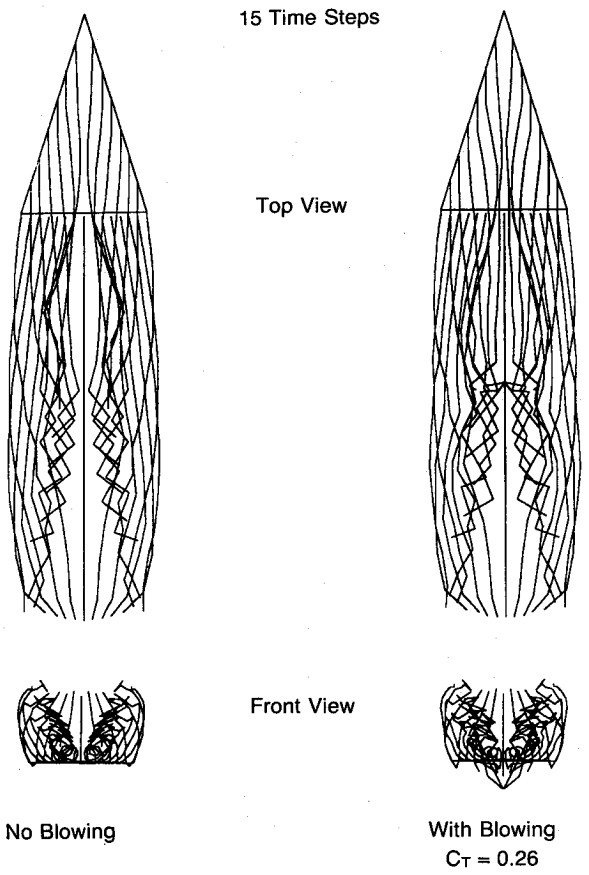

Fig. 7 Wake rollup computations with and without normal blowing.

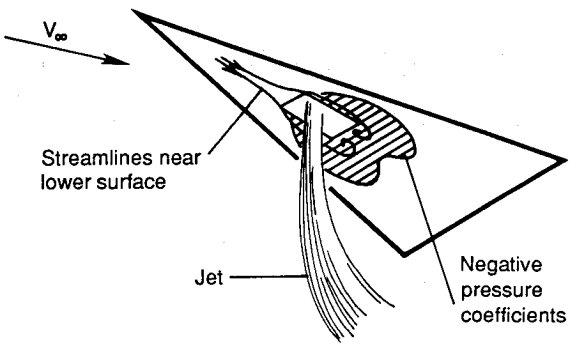

Fig. 8 Schematic description of the flowfield under the wing and near the jet.

in $C_L = 0.015$ at $\alpha = 0$), which was not accounted for by the vortex model. At the larger angle-of-attack range, the lift is considerably increased by the vortex lift, and the theoretical lift (with the leading edge vortex model) is close to the measured data. The effect of the thin, high-pressure air-supply line (without the jet but with the hole in the wing) was investigated briefly, too, and was found to be negligible.

The main objective of this study was to investigate the effect of the ejector-type flow on the wing aerodynamics at low speeds and high angles of attack. Even if the rectangular hole was not an effective ejector design, it had most features of an ejector, and a jet-induced secondary flow existed there throughout the whole experiment. Figure 6 shows that for low-speed flight conditions ($C_T > 0.2$), there is a measurable lift loss and drag loss with the ejector jet on throughout the whole range of angle-of-attack (note that both lift and drag do not include thrust components of jet). Numerical (see Fig. 7) and experimental flow visualizations (with a tuft grid) indicate that with the jet on, the leading edge vortices move inward and to a slightly lower position. However, the numerical model showed that only a small fraction of the lift loss depicted in Fig. 6 is caused by this vortex dislocation. Most of the lift loss accounted for by the numerical model is a result of the ejector being represented by a concentrated vortex ring on the wing surface. Since the trailing segment of this vortex ring was placed at the quarter chord of the panel behind the ejector opening, the lift of the panels immediately behind the jet was reduced. Similarly, the leeward segment of this vortex ring (which was placed at the quarter chord of the ejector opening and therefore did not count as "bound vortex") was to increase the potential-flow lift of the wing ahead of the jet. Since the area behind the jet is larger, the overall effect is a small reduction in the total lift.

The larger lift loss, shown by the experimental data, is a result of flow separations behind the jet and under the wing. This was observed during flow visualization with tufts on the wing and helium-filled soap bubbles seeded in the freestream (and shown schematically in Fig. 8). As the freestream flow moves around the high-momentum jet it creates two concentrated vortices behind the jet, which results in a low pressure-coefficient area under the wing (see Fig. 8). Similar flow patterns were observed in the case of a normal jet in a crossflow, and pressure coefficients on the order of -1 were measured behind the jet exit.[12-14] This can explain the larger lift loss, which is present even at $\alpha = 0$ (in Fig. 6). Such flow separation behind the jet cannot be computed by this simple vortex model, and even the portion predicted by the computation is a result of the oversimplified jet model. The analysis of the potential flow effect, however, clearly helped in identifying the various contributions to the lift loss.

Throughout the experiments, the jet parameters and thrust were held constant, and the effect of thrust coefficient C_T was investigated by varying the wind-tunnel speed (15–45 m/s). Figure 9 indicates that for low-flight speed (higher C_T), the lift loss is relatively larger. This observation is important because for actual V/STOL aircraft, the ejectors are used for landing and for low-speed maneuvers, and, if possible, any lift loss needs to be avoided. As the freestream velocity increases, (C_T reduces), and the jet-induced lift loss becomes smaller, but at this range the use of vertical ejectors is unlikely.

During the experiments, additional parameters affecting the ejector performance were investigated. Those included slightly varied ejector shapes and variations of jet-nozzle location within the ejector. These parameters had no major effect on the nature of the data reported here. As an example, the effect of varying nozzle location (height) inside the ejector is presented in Fig. 10. Because of the simple shape of the ejector,

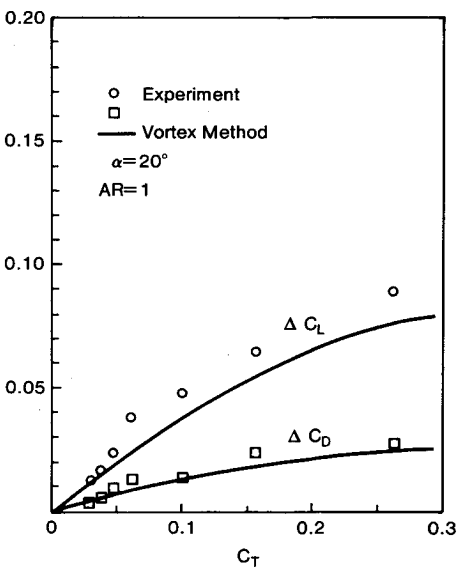

Fig. 9 Effect of thrust coefficient C_T (or flight speed) on lift and drag losses ($Re_c \approx 0.6$–1.2×10^6).

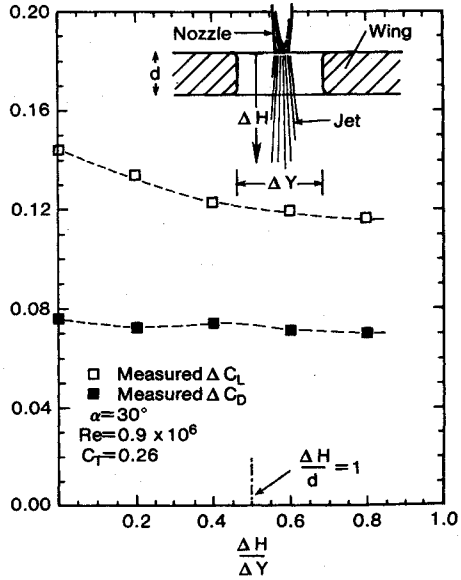

Fig. 10 Effect of jet vertical location, relative to wing, on the lift and drag losses.

ΔC_L and ΔC_D are not very sensitive to this parameter, but the effect is larger when the jet is closer to the opening in the wing ($\Delta H/\Delta Y \approx 0.5$). Throughout the experiment and for Figs. 6 and 9, this value of 0.5 was kept constant.

Conclusions

Results of this study indicate that lift loss due to ejector jets is measurable at all angles of attack. The effect is the strongest at low freestream velocities and may affect low speed and landing maneuvers of V/STOL aircraft even away from ground effect.

Combination of simplified numerical models with experimental techniques can ease the analysis of complex flowfields. This can be in the form of calculated pressure or force data or as a numerical flow visualization, as was used here.

Acknowledgments

This work was supported by NASA Ames Research Center under Grant NCC-2-458 with Dr. Larry Olson as project monitor.

References

[1]Kuhn R. E., and Eshelman J., "Ground Effects on V/STOL and STOL Aircraft-A Survey," NASA TM-86825, Nov. 1985.

[2]Aoyagi K., "Wind-Tunnel Investigation of a Large-Scale VTOL Aircraft Model With Wing Root and Wing Thrust Augmentors," NASA TM-78589, Dec. 1978.

[3]Gentry, G. L., and Margason, R. J., "Jet-Induced Lift Losses on VTOL Configurations Hovering In and Out of Ground Effect," NASA TN-D-3166, Feb. 1966.

[4]Howell, G. A., "Test Results of Chordwise and Spanwise Blowing for Low-Speed Lift Augmentation," ICAS Paper 82-5.7.1, Aug. 1982.

[5]McMahon, H. M., "Flap Surface Pressure Behind a Jet Issuing From a Wing in Cross Flow," *Proceedings of V/STOL Aircraft Aerodynamics Conference,* May 1979, pp. 191–203.

[6]Tavella, D. A., "Aerodynamics of Delta Wings with Leading Edge Blowing," AIAA Paper 86-2230, Aug. 1986.

[7]Wood, N. J., and Roberts, L., "The Control of Vortical Lift on Delta Wings By Tangential Leading Edge Blowing," AIAA Paper 87-0158, Jan. 1978.

[8]Katz, J., "Lateral Aerodynamics of Delta Wings With Leading Edge Separation," *AIAA Journal*, Vol. 22, No. 3, 1984, pp. 323–328.

[9]Katz, J., and Maskew, B., "Unsteady Low-Speed Aerodynamic Model for Complete Aircraft Configurations," *Journal of Aircraft*, Vol. 25, No. 4, 1988, pp. 302–310.

[10]Katz, J., "Calculation of the Aerodynamic Forces on Automotive Lifting Surfaces," *ASME Journal of Fluids Engineering*, Vol. 107, No. 4, 1985, pp. 438–443.

[11]Katz, J., "Evaluations of an Aerodynamic-Load Prediction Method on a STOL Fighter Configuration," AIAA Paper 86-0590, Jan. 1986.

[12]Kuhlman, J. M., Ousterhout, D. S., and Warcup, R. W., "Experimental Investigation of Effect of Jet Decay Rate on Jet-Induced Pressures on a Flat Plate," NASA CR-2979, April 1978.

[13]Shetz, J. A., Jakubowski, A. K., and Aoyagi, K., "Surface Pressures on a Flat Plate with Dual Jet Configurations," *Journal of Aircraft*, Vol. 21, No. 7, 1984, pp. 484–488.

[14]Kavasaoglu, J. A., Shetz, J. A., and Jakubowski, A. K., "Dual Rectangular Jets from a Flat Plate in a Crossflow," AIAA Paper 86-0477, Jan. 1986.